

# Investigation of the vibrational dynamics of the HCN/CNH isomers through high order canonical perturbation theory

Dominique Sugny and Marc Joyeux<sup>a)</sup>

*Laboratoire de Spectrométrie Physique, Université Joseph Fourier—Grenoble I, BP 87, 38402 St Martin d'Hères, France*

Edwin L. Sibert III<sup>b)</sup>

*Department of Chemistry and Theoretical Chemistry Institute, University of Wisconsin—Madison, Madison, Wisconsin 53706*

(Received 28 April 2000; accepted 2 August 2000)

Molecular vibrations of the molecule HCN/CNH are examined using a combination of a minimum energy path (MEP) Hamiltonian and high order canonical perturbation theory (CPT), as suggested in a recent work [D. Sugny and M. Joyeux, *J. Chem. Phys.* **112**, 31 (2000)]. In addition, the quantum analog of the classical CPT is presented and results obtained therefrom are compared to the classical ones. The MEP Hamiltonian is shown to provide an accurate representation of the original potential energy surface and a convenient starting point for the CPT. The CPT results are subsequently used to elucidate the molecular dynamics: It appears that the isomerization dynamics of HCN/CNH is very trivial, because the three vibrational modes remain largely decoupled up to and above the isomerization threshold. Therefore, the study of the three-dimensional HCN/CNH system can be split into the study of several one-dimensional bending subsystems, one for each value of the numbers  $v_1$  and  $v_3$  of quanta in the CH and CN stretches. In particular, application of high order CPT to the most precise available *ab initio* surface provides simple expressions (quadratic polynomials) for the calculation of the heights of the isomerization barrier and of the CNH minimum above the HCN minimum for each value of  $v_1$  and  $v_3$ . © 2000 American Institute of Physics. [S0021-9606(00)00441-4]

## I. INTRODUCTION

Studies of the highly excited vibrational dynamics and spectroscopy of HCP,<sup>1–3</sup> HOCl,<sup>4</sup> HCCH,<sup>5,6</sup> and DCP<sup>7</sup> have demonstrated and highlighted the complementary aspects of potential energy surfaces and resonance Hamiltonians for interpreting experimental results. In this context, a resonance Hamiltonian is one in which one or two low order resonances between the normal modes are responsible for the prominent features of the quantum and classical dynamics over a wide energy range. For example, a 1:2 Fermi resonance<sup>8,9</sup> accounts for most of the dynamics of CO<sub>2</sub>,<sup>10–17</sup> CS<sub>2</sub>,<sup>18–22</sup> substituted methane,<sup>12–14,23–25</sup> HCP,<sup>1–3</sup> DCP,<sup>7</sup> and HOCl,<sup>4</sup> while the dynamics of O<sub>3</sub> (Refs. 26–28) and H<sub>2</sub>S<sup>29</sup> is governed by a 2:2 Darling–Dennison resonance.<sup>30–32</sup> H<sub>2</sub>O is a slightly more complex case, because both the Fermi and Darling–Dennison resonances must be taken into account for an accurate description,<sup>33–35</sup> even though the principle feature, the local modes, are due to the Darling–Dennison resonance alone.<sup>13,28</sup> These Hamiltonians remain an active area of investigation, even when accurate surfaces are available, because resonance Hamiltonians have a set of good quantum numbers and classical constants of the motion explicitly built-in, whereas the only conserved quantity in global surfaces, which take all resonances into account, is energy. These conserved quantities allow, in turn, for a much simpler

and deeper study of the dynamics of the system, especially when associated with the so-called EBK (Einstein–Brillouin–Keller) semiclassical quantization rules.<sup>36–38</sup>

There are basically two methods for obtaining resonance Hamiltonians: (i) by a fit of effective parameters to a set of measured or calculated transition frequencies, and (ii) the use of high order canonical perturbation theory (CPT). There are several variants of the latter approach. They include the original quantum approach due to Van Vleck,<sup>39–45</sup> the classical method developed by Birkhoff<sup>46</sup> and later extended by Gustavson,<sup>47–49</sup> or the more recent classical procedures based on Lie algebra.<sup>50–56</sup> While a fit is often simpler to perform than CPT, the latter procedure appears more reliable whenever the perturbation expansion converges, because it avoids the plague of multiple solutions, which can never be totally banned with the fitting procedure. For this reason, this paper describes the construction of resonancelike Hamiltonians using CPT.

Until very recently, explicit high order CPT calculation schemes have been known only for motion around a single minimum, so that only rigid molecules, like CH<sub>4</sub> and its deuterated analogs,<sup>44</sup> CF<sub>4</sub>,<sup>45</sup> H<sub>2</sub>CO,<sup>57,58</sup> isotopic derivatives of water,<sup>58,59</sup> C<sub>2</sub>H<sub>2</sub>,<sup>60,61</sup> CO<sub>2</sub>,<sup>15,16,60</sup> SO<sub>2</sub>,<sup>58</sup> HCP,<sup>62</sup> or AlF<sub>3</sub> and SiF<sub>3</sub><sup>+</sup>,<sup>63</sup> could be investigated. It is to be noted that HCN has been studied,<sup>57,60,64</sup> but only far below the isomerization barrier, which occurs at about 15 000 cm<sup>-1</sup> above the ground state, so that the influence of the CNH well could safely be neglected. In contrast, we have shown recently<sup>65</sup> that CPT

<sup>a)</sup>Electronic mail: Marc.Joyeux@ujf-grenoble.fr

<sup>b)</sup>Electronic mail: sibert@chem.wisc.edu

can also be used for floppy molecules in an energy range broad enough so that more than one equilibrium position have to be taken into account. A detailed calculation scheme was provided, which was shown to work for simple models. The first purpose of the present paper is to extend that study and to demonstrate the efficiency of this procedure for realistic surfaces; we do this using the HCN/CNH as a prototype, demonstrating that a single perturbation Hamiltonian can reproduce the spectrum over a large energy range.

Having demonstrated the validity of the resonance Hamiltonian we then use it to investigate the dynamics in both the HCN and CNH wells up to and above the isomerization barrier. The surface designed many years ago by Murrell, Carter, and Halonen<sup>66</sup> (hereafter called the MCH surface), as well as the *ab initio* surface computed more recently by Bowman and co-workers<sup>67</sup> (hereafter called the BGBLD surface) will be investigated. Although not very accurate, especially at high energies, the MCH surface has nevertheless been used in most calculations performed up to date on the HCN/CNH system.<sup>68–83</sup> We studied it precisely for the sake of comparison with other approximate methods.

The principal problem one is confronted with when handling a realistic surface, instead of the simple models studied in Ref. 65, consists in obtaining a workable expansion of the initial Hamiltonian. Indeed, since explicit calculations involve repeated differentiation, CPT cannot be applied directly to the realistic surface and a more manageable approximation thereof must first be derived. As shown in Ref. 65, mixed expansions, where oscillatorlike modes (mostly stretching degrees of freedom) are expanded in polynomials and hindered-rotor-like ones (mostly bending degrees of freedom) in trigonometric functions, are well suited for the application of CPT to systems with more than one equilibrium position. Inspired by the pioneering work of Marcus, Miller and co-workers, and others,<sup>84–90</sup> we will demonstrate that expansion of the initial surface around the “reaction pathway,” or “minimum energy path,” which links the extrema of the surface, not only provides accurate potential expansions but manageable and accurate expressions for the kinetic energy. The practical calculations (gridded Taylor expansions followed by Fourier expansions), involved in the derivation of the kinetic and potential energy, will be described in some detail, because the success of the whole procedure relies thereon.

The final purpose of this paper is to provide a quantum version of the classical scheme presented in the preceding article.<sup>65</sup> In that work, Birkhoff–Gustavson CPT,<sup>46–49</sup> which consists of a series of classical canonical transformations, was applied to a classical Hamiltonian. The resulting resonance Hamiltonian was then quantized according to approximate quantization rules, such as that due to Weyl, in order to study the molecular eigenstates. In this paper we show that one can also start with a quantum Hamiltonian and apply a series of unitary transformations, in the spirit of canonical Van Vleck’s perturbation theory.<sup>39–45</sup> We consider two approaches. In the first approach, we follow a scheme similar to the one McCoy, Burleigh, and Sibert<sup>58</sup> used in rotation–vibration problems. We expand the Hamiltonian as a sum of terms that are functions of harmonic oscillator raising and

lowering operators for the stretch degrees of freedom, and the expansion coefficients are functions of the bending degrees of freedom. The stretches are then treated using Van Vleck perturbation theory, however, since the coefficients no longer commute, recurrence formulas are needed to handle the operator ordering problem, which even in the case of a single equilibrium position is of fundamental importance for practical computational purposes.<sup>44</sup> We also present a more general approach in which we express the bend dependent coefficients in a matrix representation.

The remainder of this article is organized as follows: Section II describes the derivation of the classical perturbative Hamiltonian. The expansion of the exact Hamiltonian in mixed series is presented in some detail and the ordering problem is discussed in relation with the convergence of the perturbation series. The two approaches for the quantum mechanical version of the modified CPT, which are based either on operator or matrix representations, are next developed in Sec. III. The results obtained from the classical and quantum perturbative Hamiltonians are compared at the end of the same section. Section IV contains a discussion of the dynamics of the HCN/CNH molecule in terms of the one-dimensional bending pseudopotentials derived from the perturbative Hamiltonian. At last, the complementary aspects of exact quantum calculations and perturbative ones are emphasized in Sec. V.

## II. CLASSICAL DERIVATION OF THE PERTURBATION HAMILTONIAN

We begin this section by describing our method for expanding the classical Hamiltonian about the minimum energy path in a set of coordinates that allows us to implement the perturbative transformations. Having presented the Hamiltonian, we address the issue of assigning an order to each term in the perturbative expansion. We conclude this section by presenting the results of the CPT.

### A. Expansion of the exact Hamiltonian

Defining the Jacobi coordinates  $r$ ,  $R$ , and  $\gamma$  as the interatomic CN distance, the length between  $H$  and the center of mass  $G$  of CN, and the  $HGC$  angle, respectively, the “exact” classical Hamiltonian is expressed in the form

$$H = T + V,$$

$$T = \frac{1}{2} \mu_1 p_r^2 + \frac{1}{2} \mu_2 p_R^2 + \frac{1}{2} \left( \frac{\mu_1}{r^2} + \frac{\mu_2}{R^2} \right) p_\gamma^2 + \frac{1}{2I} p_\chi^2, \quad (2.1)$$

$$V = V(r, R, \gamma).$$

Here the potential energy surface  $V(r, R, \gamma)$  is either the MCH or BGBLD surface. In the expression of the kinetic energy  $T$ ,  $\mu_1 = 1/m_C + 1/m_N$  and  $\mu_2 = 1/m_H + 1/(m_C + m_N)$ , where  $m_H$ ,  $m_C$ , and  $m_N$  are the masses of the H, C, and N atoms, respectively. The last term in the expression of  $T$  is due to the angular momentum  $p_\chi$  about the axis with least moment of inertia  $I$ , which is close to the body-fixed CN axis. Although the rotationless molecule studied in this work does satisfy  $J = p_\chi = 0$ , this term cannot be neglected because of the singularity at equilibrium. Indeed, the moment of in-

ertia  $I$  vanishes at  $\gamma=0$  and  $\gamma=\pi$ , so that  $p_\chi^2/I$  is undetermined for these values of  $\gamma$ . From the numerical point of view, the vibrational angular momentum is responsible for the fact that Legendre polynomials will be used instead of the simpler exponential basis to diagonalize the bending problem.

Although CPT can formally be applied to any kind of Hamiltonian, its use is nevertheless practically restricted to relatively simple expressions, because the calculation procedure requires repeated differentiation. In the case of rigid molecules with a single equilibrium configuration, the first step therefore consists in expanding  $T$  and  $V$  in Taylor series around the equilibrium position. In the case of systems with several equilibrium configurations, however, more sophisticated expansions must be used. Following previous work,<sup>78–81</sup> mixed polynomial/trigonometric expansions, which have been shown to work well for simpler models,<sup>65</sup> are used for the HCN/CNH system. These mixed expressions are obtained through a two-step series expansion (Taylor expansion followed by Fourier expansion) around the minimum energy path (MEP), as will now be described briefly. The MEP, which is sometimes also called the ‘‘reaction pathway,’’<sup>89–91</sup> is defined as the line on which the potential energy  $V$  is minimum with respect to the two stretching coordinates  $r$  and  $R$ . It is obtained as a set of points  $[\gamma, r_{\text{MEP}}(\gamma), R_{\text{MEP}}(\gamma)]$ , where  $r_{\text{MEP}}$  and  $R_{\text{MEP}}$  are solutions of

$$\left(\frac{\partial V}{\partial r}\right)_\gamma = \left(\frac{\partial V}{\partial R}\right)_\gamma = 0. \quad (2.2)$$

This line starts from the HCN zero-energy point, goes through the saddle located at  $12\,168\text{ cm}^{-1}$  (MCH surface) or  $16\,866\text{ cm}^{-1}$  (BGBLD surface), and then goes down to the CNH secondary minimum located at  $3911\text{ cm}^{-1}$  (MCH surface) or  $5202\text{ cm}^{-1}$  (BGBLD surface). The MEP is used to define a coordinate transformation, according to

$$\begin{aligned} \Delta r(\gamma) &= r - r_{\text{MEP}}(\gamma), \\ \Delta R(\gamma) &= R - R_{\text{MEP}}(\gamma). \end{aligned} \quad (2.3)$$

For the MCH surface,  $V$  is next expanded in a two-dimensional Taylor series with respect to  $\Delta r$  and  $\Delta R$  for a one-dimensional grid of values of  $\gamma$  ranging from  $-\pi$  to  $\pi$ , and the coefficients  $C_{p,q}(\gamma) = (\partial^{p+q} V / \partial(\Delta r)^p \partial(\Delta R)^q)_\gamma$  of the Taylor series are tabulated as a function of  $\gamma$ . At last, these tables are used to expand numerically each coefficient  $C_{p,q}$  in a Fourier series with respect to  $\gamma$ , so that the potential energy is finally rewritten in the form

$$V = \sum_{p,q,n} V_{p,q,n}(\Delta r)^p (\Delta R)^q \cos(n\gamma). \quad (2.4)$$

A similar expansion is obtained for the BGBLD potential energy surface, although a slightly different procedure is needed, because the spline interpolation along the  $R$  coordinate used by Bowman and co-workers<sup>67</sup> makes the Taylor expansion with respect to this coordinate inadequate (note that the spline interpolation along the  $\gamma$  coordinate is comparatively of little consequence since only discrete values of  $\gamma$  are used). Consequently,  $V$  is instead expanded in a one-

dimensional Taylor series with respect to  $\Delta r$  for a two-dimensional grid of points  $(\Delta R, \gamma)$  regularly spaced around the MEP. The coefficients  $C_p(\Delta R, \gamma) = (\partial^p V / \partial(\Delta r)^p)_{(\Delta R, \gamma)}$  of the Taylor series are tabulated as a function of  $\Delta R$  and  $\gamma$ . For each value of  $\gamma$ , the coefficients  $C_p$  for increasing values of  $\Delta R$  are then fitted by a polynomial in terms of  $\Delta R$ , and the fitted coefficients are tabulated as a function of  $\gamma$ . This last table is finally used to expand the fitted coefficients in Fourier series with respect to  $\gamma$ , leading to the same expansion as in Eq. (2.4). Note, however, that the exponent  $q$  in Eq. (2.4) cannot be larger than the order of the fitted polynomial for the BGBLD surface. Moreover, care was taken so as to choose the two-dimensional grid of points and the order of the fitted polynomial in a region where the final perturbation Hamiltonian remains stable upon reasonable variations thereof. The range  $-0.29 \leq \Delta R \leq 0.69$  and a sixth-order polynomial were found to be convenient.

Let us now turn to the kinetic energy. The first step consists in rewriting the vibrational angular momentum energy in the most useful form<sup>79</sup>

$$\frac{1}{2I} p_\chi^2 = \frac{1}{2} \left( \frac{\mu_1}{r^2} + \frac{\mu_2}{R^2} \right) \frac{p_\chi^2}{\sin^2 \gamma} \left( \frac{1}{2} + \sqrt{\frac{1}{4} - \frac{\sin^2 \gamma}{2 + \frac{\mu_1 R}{\mu_2 r} + \frac{\mu_2 r}{\mu_1 R}}} \right). \quad (2.5)$$

Upon expansion of Eq. (2.5) in the neighborhood of the MEP, it is clear that the only term which does not vanish everywhere for the nonrotating molecule ( $p_\chi=0$ ) is

$$\frac{1}{2} \left( \frac{\mu_1}{r^2} + \frac{\mu_2}{R^2} \right) \frac{p_\chi^2}{\sin^2 \gamma}, \quad (2.6)$$

due to the singularity at  $\gamma=0$ . The coefficient in front of  $p_\chi^2/\sin^2 \gamma$  in Eq. (2.6) is the same as the coefficient in front of  $p_\gamma^2$  in Eq. (2.1). The kinetic energy for the nonrotating molecule can therefore be rewritten in terms of the momenta  $p_{\Delta R}$ ,  $p_{\Delta r}$ ,  $p_\gamma$ , and  $p_\chi$  conjugate to  $\Delta r$ ,  $\Delta R$ ,  $\gamma$  and  $\chi$ , respectively, in the form

$$\begin{aligned} T &= \frac{1}{2} \mu_1 p_{\Delta r}^2 + \frac{1}{2} \mu_2 p_{\Delta R}^2 + \frac{1}{2} \left( \frac{\mu_1}{r^2} + \frac{\mu_2}{R^2} \right) \\ &\times \left( \left( p_\gamma - \frac{\partial r_{\text{MEP}}}{\partial \gamma} p_{\Delta r} - \frac{\partial R_{\text{MEP}}}{\partial \gamma} p_{\Delta R} \right)^2 + \frac{p_\chi^2}{\sin^2 \gamma} \right). \end{aligned} \quad (2.7)$$

The above-described procedure for expanding the potential energy in the neighborhood of the MEP is next applied to each one of the six coefficients in front of  $p_{\Delta r}^2, p_{\Delta R}^2, \dots$ , so that kinetic energy is finally rewritten in the form

$$\begin{aligned} T &= \sum_{p,q,n} (\Delta r)^p (\Delta R)^q \cos(n\gamma) \left\{ T_{p,q,n}^{(1)} p_{\Delta r}^2 + T_{p,q,n}^{(2)} p_{\Delta R}^2 \right. \\ &\quad \left. + T_{p,q,n}^{(3)} \left( p_\gamma^2 + \frac{p_\chi^2}{\sin^2 \gamma} \right) + T_{p,q,n}^{(4)} p_{\Delta r} p_{\Delta R} \right\} \\ &\quad + \sum_{p,q,n} (\Delta r)^p (\Delta R)^q \sin(n\gamma) \\ &\quad \times \left\{ T_{p,q,n}^{(5)} p_{\Delta r} p_\gamma + T_{p,q,n}^{(6)} p_{\Delta R} p_\gamma \right\}. \end{aligned} \quad (2.8)$$

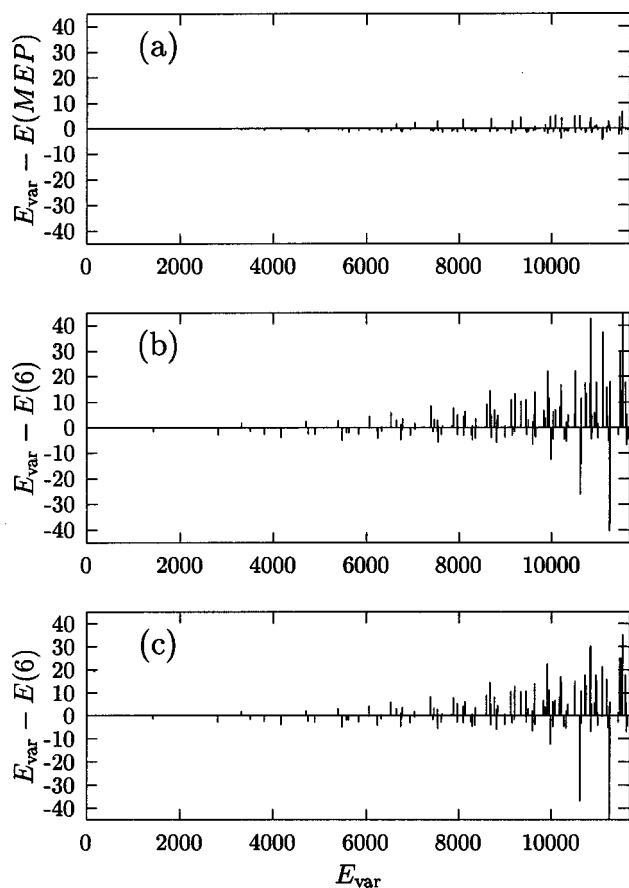


FIG. 1. Energy difference between the variational energies reported by Basic for the first 111 states of the MCH surface (Ref. 66) and (a) those of the mixed expansion in Eqs. (2.4) and (2.8), (b) those obtained from sixth-order quantum canonical perturbation theory, and (c) those of Eq. (2.9) obtained from sixth-order classical canonical perturbation theory.

It should be noted that the derivatives of  $r_{\text{MEP}}$  and  $R_{\text{MEP}}$  with respect to  $\gamma$  need only be known at discrete values of  $\gamma$ , so that explicit expressions for these functions are not required. The derivatives are instead calculated numerically, together with the values of  $r_{\text{MEP}}$  and  $R_{\text{MEP}}$ , as the MEP is determined at the very beginning of the procedure.

It is worthwhile to test the accuracy of this expansion. This allows us to test the combined effects of the classical MEP transformations and the expansion of the potential. We do this by variationally calculating, for the MCH surface, the eigenvalues of the Hamiltonian of Eqs. (2.4) and (2.8) and comparing them to those of Basic.<sup>75</sup> The results are given in Fig. 1(a). Below 7000  $\text{cm}^{-1}$  above the zero-point energy the largest difference is 2  $\text{cm}^{-1}$  and below 11 700  $\text{cm}^{-1}$ , the largest error is 5  $\text{cm}^{-1}$ . In general, however, the error is much smaller. A key step in this comparison is obtaining the eigenvalues of the classical Hamiltonian. This step is described in Sec. III.

## B. The ordering problem

Having obtained the expansions of Eqs. (2.4) and (2.8), one must assign an order to each term and apply CPT in order to put the perturbation Hamiltonian in the form

$$H = \sum_{k,l,m,n} a_{k,l,m,n} I_1^k I_3^l \left( p_2^2 + \frac{p_x^2}{\sin^2 q_2} \right)^m \cos(nq_2), \quad (2.9)$$

where the indices 1–3 describe the CN-stretch, the bend, and the CH-stretch normal modes, respectively, and  $I_k$  is the action integral of the  $k$ th ( $k=1,3$ ) normal mode

$$I_k = \frac{1}{2} (p_k^2 + q_k^2). \quad (2.10)$$

Note that the coordinates for the stretch degrees of freedom (modes 1 and 3) are dimensionless normal coordinates, while the coordinate  $q_2$  is an anglelike coordinate expressed in radians. The numerical values for the  $a_{k,l,m,n}$  parameters in Eq. (2.9) are too lengthy to reproduce here, however they are available on the World Wide Web at <http://www.chem.wisc.edu/~sibert/hcn> or by request to one of the authors.

The expression in Eq. (2.9) is obtained under the assumption that all of the nonlinear resonances between the three normal modes are negligible. The numerical results presented in the following show that this assumption is valid in the case of HCN/CNH, at least up to the isomerization barrier and within the accuracy of a few  $\text{cm}^{-1}$  (see the following). For higher energy values or better precision, it might be necessary to take one or several resonances into account, as in Ref. 92, which leads to somewhat more complex expressions. It is nevertheless interesting to notice that the Hamiltonian in Eq. (2.9) is formally very close to the resonance Hamiltonians mentioned in Sec. I, in that it depends on a single angle, namely  $q_2$ . However, this angular dependence is due here to the need to take into account two wells instead of a resonance between two normal modes. Let us further note, that for quantum mechanical purposes, each classical term is symmetrized according to Weyl's rule

$$\begin{aligned} & \left( p_2^2 + \frac{p_x^2}{\sin^2 q_2} \right)^m \cos(nq_2) \\ & \rightarrow \frac{1}{2^{2m}} \sum_{k=0}^{2m} \binom{m}{k} \left( \left( p_2^2 + \frac{p_x^2}{\sin^2 q_2} \right)^{k/2} \right. \\ & \quad \left. \times \cos(nq_2) \left( p_2^2 + \frac{p_x^2}{\sin^2 q_2} \right)^{m-k/2} \right). \end{aligned} \quad (2.11)$$

(For a good discussion of the problems raised by the quantization and symmetrization of a classical Hamiltonian, see e.g., Ref. 93.)

The reader is referred to the preceding article<sup>65</sup> for the explicit application of classical CPT and to Sec. III for a description of the quantum version of it. The ordering problem will nevertheless be discussed here in more detail, because the statements made in Ref. 65 need be somewhat moderated. The major statement in Ref. 65 is that the lowest order term  $H_0$  of the Hamiltonian must contain only the sum of the quadratic terms dealing with the oscillatorlike degrees of freedom (here the two stretching modes). This point is absolutely compulsory<sup>65</sup> so that, for the HCN/CNH system,  $H_0$  is defined as the sum of the terms with  $V_{2,0,0}$ ,  $V_{0,2,0}$ , and  $V_{1,1,0}$  in Eq. (2.4), plus the terms with  $T_{0,0,0}^{(1)}$  and  $T_{0,0,0}^{(2)}$  in Eq. (2.8). It was next suggested in Ref. 65 that all of the other



terms of the Hamiltonian be put in  $H_1$ , in order to avoid possible errors due to an improper ordering. Although a good suggestion for the simpler models handled in Ref. 65, this proved to be unmanageable for the HCN/CNH system, because the calculations far exceed our (modern) computer capabilities.

The problematic aspect of the ordering is for the terms dealing with the hindered-rotor-like modes (here the bending degree of freedom), because the terms  $V_{p,q,n} \cos(n\gamma)$  do not monotonously decrease with increasing values of  $n$ . In contrast, the usual ordering of CPT is expected to work for the two stretching degrees of freedom. Therefore, an order 2 was arbitrarily assigned to all of the  $\cos(n\gamma)$  terms, each monome with total degree  $n+2$  was put in  $H_n$ , and all the spurious terms in  $H_0$  (cf. the previous paragraph) were moved from  $H_0$  to  $H_1$ . This ordering, which lies halfway between the almost total lack of ordering suggested in the preceding article<sup>65</sup> and the too rigid ordering assumed in the torsional problem,<sup>94–101</sup> has the merit to fulfill all the requirements: The ordering of bending terms is avoided, computer time and memory needs are strongly reduced, and quantum mechanical calculations are numerically stable as the size of the basis of Legendre polynomials for the bend degree of freedom is increased from 51 to 71.

The last point to be tackled is that of the length of the Fourier transforms. In particular, what is the maximum value  $n_{\max}$  of  $n$  in Eqs. (2.4) and (2.8)? It turns out that the HCN/CNH results are improved when  $n_{\max}$  is increased up to about 18. Results then remain stable for larger values of  $n_{\max}$ . Therefore, all the classical numerical results presented in this article were obtained with  $n_{\max}=18$ . Moreover, it proved to be important in the course of calculations to drop all the terms with  $n$  larger than  $n_{\max}$  in order, once more, to keep the number of terms in the perturbation calculations manageable. It was thoroughly checked that this truncation has a negligible effect on the final results.

### C. Results

We are now in the position to check the accuracy of the perturbation scheme through the comparison of levels obtained by replacing  $I_1$  and  $I_3$  by  $v_1+1/2$  and  $v_3+1/2$ , respectively, in Eqs. (2.9)–(2.11) with those obtained from exact quantum calculations. The comparison obviously deals with levels that have been assigned the same quantum numbers  $v_1$ ,  $v_2$ , and  $v_3$ . While the assignment procedure might be somewhat tedious for exact quantum states, it is very simple for the perturbation ones, because the numbers  $v_1$  and  $v_3$  of quanta in the two stretching degrees of freedom remain good quantum numbers. Therefore, one only has to inspect visually one-dimensional wave functions and to count the number of nodes along the  $q_2$  coordinate between 0 and  $\pi$  in order to assign the last quantum number  $v_2$  and the localization flag (localized in the HCN well, localized in the CNH well, or delocalized). This point is clearly illustrated in Fig. 2, which displays the probability as a function of  $q_2$  for the states with  $v_1=v_3=0$  in the MCH surface, the baseline for each plot being located (on the vertical axis) at the energy of the state. It is worth noting that the assignment of states obtained from our perturbative Hamiltonian is absolutely not

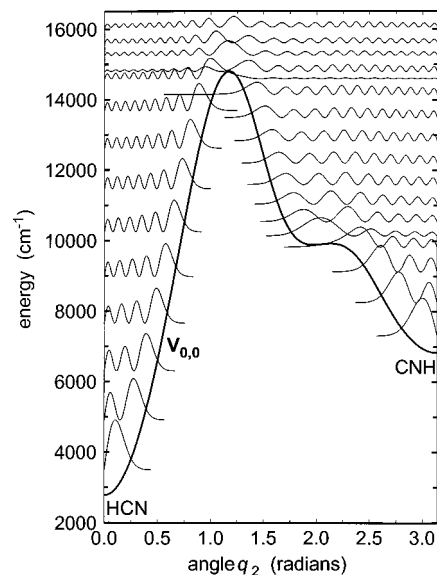


FIG. 2. Plot, as a function of  $q_2$ , of the  $V_{0,0}$  pseudopotential and the probabilities  $|\Psi(q_2)|^2 \sin(q_2)$  for the complete spectrum with  $v_1=v_3=0$ , according to the plot of  $V_{0,0}$  and are given relative to the minimum of the potential energy surface. The scale is the same for all the probability plots and the baseline for each plot coincides, on the vertical axis, with the energy of the state. Note that the probability is zero at  $q_2=0$  and  $q_2=\pi$  because of the  $\sin(q_2)$  term, although  $q_2=0$  and  $q_2=\pi$  are not nodes of the wave function  $\Psi(q_2)$ . Therefore, 0 and  $\pi$  must not be taken into account for the assignment of the levels, which just amounts to counting the number of nodes.

affected by the “shoulder” (actually a second shallow minimum) in the CNH well (see Fig. 2), whereas the presence of this shoulder prevented the study of the CNH well in Ref. 77 and limited it to the energy range below the energy of the shoulder in Ref. 81.

Concerning the MCH surface, the most comprehensive and reliable list of assigned quantum levels published up to date is that of Bacic.<sup>75</sup> This list contains all the states below  $11\,770\text{ cm}^{-1}$  above the ground state (111 states), regardless of whether they are localized in the HCN or CNH wells or delocalized over the two wells. The list contains two such states with  $v_1=v_3=0$ . At fourth order of theory, the rms and maximum errors between exact and perturbation calculations are  $30.6$  and  $77.4\text{ cm}^{-1}$ , respectively, for these 111 levels. The errors change to  $22.4$  and  $82.5\text{ cm}^{-1}$  at fifth order, and  $9.4$  and  $50.6\text{ cm}^{-1}$  at sixth order. At higher orders, the asymptotic perturbation series diverges and the errors increase. Note that such a divergence is a common property to all of the asymptotic series. Moreover, with the exception of few trivial cases, it is impossible to predict *a priori* (i.e., prior to performing the calculations) at what order the series starts to diverge and one just has to hope, as for HCN/CNH and the cases studied in Refs. 15, 16, 44, 45, 57–64, that it converges up to a sufficiently high order for the perturbative expression at that order to be sufficiently precise. As was also observed in the simpler models presented in Ref. 65, most of the average error is due to a very limited number of states. For example, if states 81, 86, 98, and 104, which are assigned as  $(0,22,0)_{\text{CNH}}$ ,  $(1,16,0)_{\text{CNH}}$ ,  $(0,44,0)_{\text{D}}$  and  $(0,14,1)_{\text{HCN}}$ , respectively, are not taken into account, then

the rms error at sixth order drops down to  $5.9 \text{ cm}^{-1}$  and the maximum one to  $20.9 \text{ cm}^{-1}$ . As in Ref. 65, these larger errors observed for a few states are due to small resonances, which are not taken into account by the perturbation Hamiltonian (see Sec. V). The perturbation Hamiltonian is accurate enough to confirm, for example, that levels 76, 80, 106, and 110 must be assigned to  $(3,6,0)_{\text{HCN}}$ ,  $(0,6,2)_{\text{HCN}}$ ,  $(3,8,0)_{\text{HCN}}$ , and  $(0,8,2)_{\text{HCN}}$ , respectively, as proposed by Bentley, Huang, and Wyatt,<sup>77</sup> whereas a reliable assignment could not be arrived at in Ref. 75. Moreover, level 98 is without any doubt a delocalized state with 44 quanta in the bending degree of freedom.

An indication of how the perturbation Hamiltonian performs at higher energies is provided by a comparison with the exact states computed by Bentley, Huang, and Wyatt.<sup>77</sup> This study reports eigenvalues up to  $22\,000 \text{ cm}^{-1}$  above the quantum ground state. It turns out that the average and maximum errors at sixth order of perturbation for the 56 levels computed between  $12\,000$  and  $16\,000 \text{ cm}^{-1}$  above the ground state are not larger than  $16.1$  and  $47.3 \text{ cm}^{-1}$ . These errors increase up to  $28.1$  and  $73.5 \text{ cm}^{-1}$  for the 69 levels between  $16\,000$  and  $20\,000 \text{ cm}^{-1}$  but are still not larger than  $43.2$  and  $104.8 \text{ cm}^{-1}$  for the next 44 levels between  $20\,000$  and  $22\,000 \text{ cm}^{-1}$ . These unexpectedly good results must however be put in perspective, since all of the levels reported by Bentley, Huang, and Wyatt<sup>77</sup> are localized in the HCN well, whereas larger errors might be expected for the delocalized states, which have a larger number of quanta in the bending degree of freedom.

At last, let us point out that CPT is much simpler than the so-called “weak-mode representation,”<sup>78–83</sup> whereas our results are nevertheless more accurate (by one to two orders of magnitude) than those reported in Refs. 78–83. If we understand this work correctly, this might be due principally to the fact that the expansion orders used by these authors are too small. CPT is also much more accurate than the adiabatic approximation in the discrete variable representation,<sup>74</sup> and as accurate as the same approximation, once nonadiabatic corrections have been performed<sup>74</sup>—with the advantage that two good quantum numbers are explicitly built-in from the very beginning.

For the BGBLD surface, states obtained from the perturbation Hamiltonian were compared to the first 175 exact quantum states up to  $14\,984 \text{ cm}^{-1}$  above the ground state reported in Tables II and III of Ref. 67 (be careful, however, as there are some misprints in these tables). This list comprises all the states in the HCN and CNH wells up to the first delocalized state. At fourth and fifth order of perturbation theory, the rms and maximum errors are  $38.0$  and  $144.6 \text{ cm}^{-1}$ , and  $33.8$  and  $135.1 \text{ cm}^{-1}$ , respectively. At sixth order, the perturbation expansion diverges and the errors increase. Once again, the accuracy of the perturbation Hamiltonian is satisfying good, especially as it can be estimated that the greatest part of the error arises from the fitting procedure used to replace the spline interpolation.

### III. QUANTUM MECHANICAL VERSION OF THE MODIFIED CPT

The quantum mechanical version of the perturbative treatment of the molecular vibrations is based on Van Vleck perturbation theory. We take as our starting point the Hamiltonian of Eqs. (2.4) and (2.8). As such we have not attempted to implement the quantum analog of the expansion about the MEP. This greatly simplifies the perturbative calculation, yet allows us to test the accuracy of the perturbative aspect of the calculation, which is the focus of this section of the paper. To obtain the initial quantum Hamiltonian, we rewrite the classical Hamiltonian for  $J=0$  in terms of the coordinate  $z = \cos(\gamma)$  and its conjugate momentum  $p_z$ , setting  $p_x = 0$ . This transformation leads to a unitary Jacobian. We then set  $p_z = -i\hbar \partial / \partial z$ . This approximate procedure leads to a non-Hermitian Hamiltonian, so the resulting Hamiltonian must be symmetrized according to Weyl’s rule [cf. Eq. (2.11)] discussed in Sec. II B, where this procedure produces a Hermitian Hamiltonian. Two simple examples, which illustrate the net effect of these transformations, are

$$p_\gamma^2 \Rightarrow -\hbar^2 \frac{\partial}{\partial z} (1-z^2) \frac{\partial}{\partial z} = \hat{T},$$

$$p_\gamma \sin \gamma \Rightarrow \frac{i\hbar}{2} \left\{ (1-z^2) \frac{\partial}{\partial z} + \frac{\partial}{\partial z} (1-z^2) \right\}. \quad (3.1)$$

As discussed in Sec. II, the eigenvalues of this final quantum Hamiltonian are compared to those of Basic<sup>75</sup> in Fig. 1(a). As this figure demonstrates, the combined errors introduced in using the classical MEP Hamiltonian, described in Sec. II, and the classical to quantum transformations, described in this section, lead to errors that are sufficiently small that for this study it is not worth trying to calculate the small quantum corrections that a more rigorous treatment would provide.

As in the classical calculations, the Hamiltonian is expanded as

$$\hat{H} = H_0 + \lambda H_1 + \lambda^2 H_2 + \dots, \quad (3.2)$$

where the order of terms follows the scheme described in Sec. II B. The Hamiltonian, as given by Eq. (3.2), is the starting point for the quantum calculations. It is transformed using Van Vleck perturbation theory following the approach that McCoy, Burleigh, and Sibert implemented in their treatment of rotation–vibration interactions.<sup>58</sup> Following that work the  $H_\nu$  are expanded as

$$H_\nu = \sum_{\mathbf{m}} \sum_{\mathbf{n}} C_{\mathbf{mn}}^{(\nu)} (a_1^+)^{m_1} (a_1)^{n_1} (a_3^+)^{m_3} (a_3)^{n_3}, \quad (3.3)$$

where  $\mathbf{m} = (m_1, m_3)$  and  $\mathbf{n} = (n_1, n_3)$  (the indexes 1 and 3 refer to the stretching degrees of freedom). This is the same form as is used in a pure vibrational problem, however, in the rotation–vibration study the expansion coefficients  $C_{\mathbf{mn}}^{(\nu)}$  are functions of the angular momentum raising and lowering operators. Hence in carrying out the transformations, McCoy, Burleigh, and Sibert<sup>58</sup> followed the same procedure as for the purely vibrational problem, with the caveat that they needed to incorporate the noncommutativity of the expansion

coefficients into the Van Vleck transformations. This was most conveniently achieved by expressing the angular momentum operators as harmonic oscillator raising and lowering operators following the work of Schwinger.<sup>102</sup>

In the present study we considered two approaches that follow the general outline of the work of McCoy, Burleigh, and Sibert.<sup>58</sup> In the first approach the  $C_{\mathbf{mn}}^{(\prime)}$  are expressed as functions of the bending degree of freedom. More specifically

$$C_{\mathbf{mn}}^{(\prime)} = \sum_{i=1}^{M_z} \sum_{j=1}^{M_p} c_{\mathbf{mn}}^{(\prime)ij} z^i \frac{\partial^j}{\partial z^j}. \quad (3.4)$$

This format has the advantage that, in the commutator algebra required in Van Vleck perturbation theory, one needs to take products of terms of the above form and then reorder them back into the original form using

$$z^m \frac{\partial^n}{\partial z^n} z^{m'} \frac{\partial^{n'}}{\partial z^{n'}} = \sum_{k=0}^{\min(m',n)} \frac{n!m'!}{k!(n-k)!(m'-k)!} \times z^{m'+m-k} \frac{\partial^{n'+n-k}}{\partial z^{n'+n-k}}. \quad (3.5)$$

As in the classical perturbation theory, the final Hamiltonian has the same form as the original Hamiltonian in Eq. (3.2) but now, in analogy to Eq. (2.9), we have

$$H_{\prime} = \sum_{\mathbf{m}} D_{\mathbf{mn}}^{(\prime)} (a_1^+)^{m_1} (a_1)^{m_1} (a_3^+)^{m_3} (a_3)^{m_3}. \quad (3.6)$$

Equation (3.6) gives the bend Hamiltonian for each set of the  $m_1$  and  $m_3$  quantum numbers. As such our approach is similar in spirit to the method of mixed diagonalization, introduced by Hernandez,<sup>103</sup> in which one constructs an effective Hamiltonian operator acting on a reduced dimensional space using the similarity transformations of canonical Van Vleck perturbation theory.

In principle, the eigenvalues of the Hamiltonian of Eq. (3.6) are most easily determined in a Legendre basis. It should be noted, however, that it was necessary to reorder the above bend terms; so instead of the terms  $D_{\mathbf{mn}}^{(\prime)}$  consisting of a sum of terms of the form of Eq. (3.4), they are expressed as

$$D_{\mathbf{mn}}^{(\prime)} = \sum_{i,j} d_{\mathbf{mn}}^{(\prime)ij} (z^i \hat{T}^j + \hat{T}^j z^i), \quad (3.7)$$

where  $\hat{T}$  is defined in Eq. (3.1). This form leads to trivial expressions for the matrix elements, since the matrix elements of  $\hat{T}$  are diagonal with respect to the Legendre basis.

The second approach is to expand the  $C_{\mathbf{mn}}^{(\prime)}$  of Eq. (3.3) in a matrix representation for the bending degree of freedom as

$$C_{\mathbf{mn}}^{(\prime)} = \sum_{i=1}^M \sum_{j=1}^M |i\rangle c_{\mathbf{mn}}^{(\prime)ij} \langle j|. \quad (3.8)$$

This representation has the advantage that the reordering of terms is replaced by matrix multiplication. Although in principle our result is independent of the representation, we find

that the number of terms  $M$  required in the expansion of Eq. (3.8) does depend on the representation. We have chosen to work with  $|i\rangle$  that are eigenfunctions of the pure bend part of the Hamiltonian contained in  $H_1$ . The  $M=36$  lowest energy bend eigenfunctions obtained using a basis of 65 Legendre functions is sufficient.

Comparing the two methods of Eq. (3.4) and Eq. (3.8), we find that the fourth-order results are independent of whether we use the operator or the matrix approach. However, at sixth order we find that the operator approach is unstable. We are not sure why instabilities arise. However, the matrix elements of terms  $z^i \partial^j / \partial z^j$  evaluated in a Legendre basis are extremely difficult to calculate due to large round off errors. It was for this reason that the terms needed to be ordered as in Eq. (3.7).

The comparison of the sixth-order quantum and classical perturbative results are shown in Figs. 1(b) and 1(c), respectively. Numerical results for states with zero quanta in the stretch degrees of freedom are shown in Table I. Given the similar levels of agreement, as demonstrated by the figures, we conclude that the quantum corrections are small compared to the convergence of the perturbative expansions. This comparison is complicated by that fact that the classical limit of the quantum perturbation theory is a Lie transform, and in the presence of resonances Lie transforms and Birkhoff–Gustavson do not yield equivalent results. Hence the differences between Figs. 1(b) and 1(c) arise from both quantum corrections and the differences between Birkhoff–Gustavson versus Lie transforms. There is no reason those two approaches should give the same answer. In systems where there is weaker stretch–bend coupling, and thus better convergence in the perturbative treatment, one can argue that one should include the quantum corrections, however, in the present case, this is clearly not true. Thus the remainder of the paper focuses entirely on the results of the Birkhoff–Gustavson CPT.

#### IV. THE VIBRATIONAL DYNAMICS OF HCN/CNH

The purpose of this section is to interpret the features observed in the quantum spectrum on the basis of the quantum-classical correspondence. Although the wave functions of the perturbation Hamiltonian in Eqs. (2.9)–(2.11) will be used for the purpose of illustration, recent work<sup>1–4,7</sup> confirms that the wave functions obtained from exact quantum calculations display the same features as the perturbation ones. Therefore, one can be confident that the conclusions, drawn for the perturbation Hamiltonian, hold for the *ab initio* surface. The two tools, which will be used extensively throughout this section, are (i) the Einstein–Brillouin–Keller (EBK) semiclassical quantization rules,<sup>36–38</sup> and (ii) classical one-dimensional (1D) pseudopotentials.

##### A. Semiclassical quantization rules and 1D pseudopotentials

The EBK semiclassical quantization rules state that, for an integrable system, each quantum state is associated with a classical trajectory (called a “quantizing” trajectory) with quantized action integrals (action integrals can be understood as generalized momenta, which remain constant along clas-

TABLE I. Energy values of the pure bending states ( $v_1=v_3=0$ ) of HCN/CNH up to  $11\,770\text{ cm}^{-1}$  above the ground state, according to the MCH surface (Ref. 66). The variational values computed by Bacic (Ref. 75) are reported in column 7. The values obtained from sixth-order semiclassical (SC) and quantum mechanical (QM) canonical perturbation theory are reported in columns 5 and 6, respectively. The labels HCN, CNH, and D in column 4 indicate whether the state is localized in the HCN well or the CNH well or is delocalized over the two wells.

$v_1$	$v_2$	$v_3$	Well	SC energy ( $\text{cm}^{-1}$ )	QM energy ( $\text{cm}^{-1}$ )	Bacic ( $\text{cm}^{-1}$ )	Bacic-SC ( $\text{cm}^{-1}$ )	Bacic-QM ( $\text{cm}^{-1}$ )
0	0	0	HCN	0.00	0.00	0.00	0.00	0.00
0	2	0	HCN	1 419.70	1 418.87	1 418.30	-1.40	-0.57
0	4	0	HCN	2 809.20	2 807.78	2 806.40	-2.80	-1.38
0	0	0	CNH	3 810.50	3 809.53	3 808.00	-2.50	-1.53
0	6	0	HCN	4 164.80	4 162.43	4 160.90	-3.90	-1.53
0	2	0	CNH	4 753.19	4 752.79	4 750.90	-2.29	-1.89
0	8	0	HCN	5 482.21	5 477.94	5 477.30	-4.91	-0.64
0	4	0	CNH	5 627.12	5 627.19	5 625.30	-1.82	-1.89
0	6	0	CNH	6 326.97	6 328.72	6 327.50	0.53	-1.22
0	8	0	CNH	6 645.97	6 647.41	6 649.30	3.33	1.89
0	10	0	HCN	6 754.75	6 748.42	6 750.00	-4.75	1.58
0	10	0	CNH	7 048.40	7 045.56	7 047.80	-0.60	2.24
0	12	0	CNH	7 540.27	7 535.46	7 538.50	-1.77	3.04
0	12	0	HCN	7 973.97	7 965.81	7 971.20	-2.77	5.39
0	14	0	CNH	8 096.86	8 089.33	8 093.80	-3.06	4.47
0	16	0	CNH	8 701.45	8 692.04	8 697.50	-3.95	5.46
0	14	0	HCN	9 128.19	9 118.11	9 129.00	0.81	10.89
0	18	0	CNH	9 340.87	9 330.36	9 340.90	0.03	10.54
0	20	0	CNH	10 000.00	9 989.05	9 987.60	-12.4	-1.45
0	16	0	HCN	10 195.40	10 185.11	10 202.20	6.80	17.09
0	22	0	CNH	10 656.70	10 645.80	10 619.80	-36.90	-26.00
0	42	0	D	11 099.40	11 099.02	11 099.00	-0.40	-0.02
0	44	0	D	11 308.40	11 297.97	11 257.70	-50.70	-40.27

sical trajectories). More precisely, for the perturbation Hamiltonian in Eqs. (2.9)–(2.11), the quantizing trajectory associated with the  $(v_1, v_2, v_3)$  quantum state satisfies

$$I_1 = v_1 + \frac{1}{2},$$

$$\mathfrak{J}_2 = \frac{1}{2\pi} \oint_{q_2 \in [-\pi, \pi]} p_2 dq_2 = v_2 + 1, \quad (4.1)$$

$$I_3 = v_3 + \frac{1}{2},$$

where  $I_1$  and  $I_3$ , which appear in Eq. (2.9), are defined in Eq. (2.10). Finding the quantizing trajectory associated with the quantum state  $(v_1, v_2, v_3)$  therefore amounts to replacing  $I_1$  and  $I_3$  with  $v_1 + 1/2$  and  $v_3 + 1/2$  in Eq. (2.9) and in searching for the energy, such that the path integral of  $p_2 dq_2$  between  $-\pi$  and  $\pi$  is equal to  $v_2 + 1$ . Because there are two wells, located around the HCN and CNH equilibrium configurations, respectively, this search leads most of the time (for localized states) to two solutions, which differ widely in their initial conditions.

Upon combination of the expression of the Hamiltonian in Eq. (2.9) with the EBK quantization rules in Eq. (4.1), it is seen that the full three-dimensional problem can be split into one 1D problem for each pair of stretching quantum numbers  $(v_1, v_3)$ : The particle with position and momentum coordinates  $q_2$  and  $p_2$ , respectively, is considered to move in a pseudopotential  $V_{v_1, v_3}(q_2)$ , with a pseudo-kinetic energy  $T_{v_1, v_3}(p_2, q_2)$ , where

$$V_{v_1, v_2}(q_2) = \sum_{k, l, n} a_{k, l, 0, n} \left( v_1 + \frac{1}{2} \right)^k \left( v_3 + \frac{1}{2} \right)^l \cos(nq_2),$$

$$T_{v_1, v_2}(p_2, q_2) = \sum_{k, l, m \neq 0, n} a_{k, l, m, n} \left( v_1 + \frac{1}{2} \right)^k \left( v_3 + \frac{1}{2} \right)^l \quad (4.2)$$

$$\times \left( p_2^2 + \frac{p_x^2}{\sin^2 q_2} \right)^m \cos(nq_2).$$

The  $p_x^2/\sin^2 q_2$  term is conserved in the right-hand side of the second equation in Eq. (4.2), despite the fact that only the rotationless molecule ( $p_x=0$ ) is studied, in order to remember that the basis of the Legendre polynomials must be used in quantizing the bend degree of freedom. It is to be noted that the pseudopotential defined in Eq. (4.2) is formally close to the effective bending potentials defined in the adiabatic approximation in the discrete variable representation.<sup>74</sup>

## B. Quantum wave functions versus pseudopotentials

It will now be shown that the features observed in quantum wave functions can be interpreted in terms of the pseudopotentials. Let us first look back at Fig. 2, where the probability for the bending states ( $v_1=v_3=0$ ) of the MCH surface and the corresponding  $V_{0,0}(q_2)$  pseudopotential have been superposed. As expected, the pseudopotential displays two principal minima, associated with the linear HCN and CNH configurations, respectively, separated by a maximum. The increase in the probability close to the classical turning



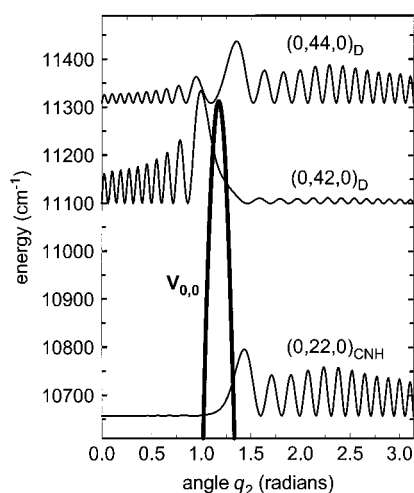


FIG. 3. Plot, as a function of  $q_2$ , of the  $V_{0,0}$  pseudopotential and the probabilities  $|\Psi(q_2)|^2 \sin(q_2)$  for the states  $(0,22,0)_{\text{CNH}}$ ,  $(0,42,0)_{\text{D}}$ , and  $(0,44,0)_{\text{D}}$ , according to the MCH surface. Energy values on the left-hand scale refer to the plot of  $V_{0,0}$  and are given relative to the quantum ground state.  $(0,22,0)_{\text{CNH}}$ ,  $(0,42,0)_{\text{D}}$ , and  $(0,44,0)_{\text{D}}$  are computed at 10 656.7, 11 099.0, and 11 309.1  $\text{cm}^{-1}$  above the ground state, respectively, according to the perturbation Hamiltonian in Eq. (2.9). All the probability plots are at the same scale. For each plot, the baseline coincides, on the vertical axis, with the energy of the state.

point and the exponential decrease in the classically forbidden region are clearly seen for all of the localized states. On the other hand, delocalized states display a larger probability at the barrier as expected due to their low kinetic energy.

A blow-up of the same figure in the energy range close to the top of the barrier is presented in Fig. 3. The last three levels below the barrier are represented. They are assigned as  $(0,22,0)_{\text{CNH}}$ ,  $(0,42,0)_{\text{D}}$ , and  $(0,44,0)_{\text{D}}$ , where the HCN, CNH, and D indices mean that the state is localized in the HCN or CNH well, or delocalized, respectively. While  $(0,22,0)_{\text{CNH}}$ , which lies  $655 \text{ cm}^{-1}$  below the barrier, is completely localized in the CNH well,  $(0,42,0)_{\text{D}}$ , which lies  $213 \text{ cm}^{-1}$  below the barrier, is clearly delocalized because of a small tunneling effect. The tunneling effect is so strong for  $(0,44,0)_{\text{D}}$ , which lies only  $4 \text{ cm}^{-1}$  below the barrier, that its probability is very similar to that of a state located above the barrier. At this point, it is worth emphasizing that tunneling-induced delocalization depends critically on the relative positions of the states in the HCN and CNH wells and might be efficient more than  $1000 \text{ cm}^{-1}$  below the barrier. For example, the probability for the states  $(4,16,0)_{\text{HCN}}$ ,  $(4,20,0)_{\text{CNH}}$ , and  $(4,22,0)_{\text{CNH}}$  is plotted in Fig. 4, together with the corresponding  $V_{4,0}$  pseudopotential. The tunneling effect is so small for  $(4,22,0)_{\text{CNH}}$ , which is located  $702 \text{ cm}^{-1}$  below the barrier, that it is best assigned as a localized state. Somewhat unexpectedly, tunneling is much more important for the two other states, which lie as far as  $1389$  and  $1401 \text{ cm}^{-1}$  below the barrier. These later states might as well be described as delocalized ones. Such a strong tunneling effect so far below the top of the barrier is due to the fact that the two states are almost degenerate, their separation being as small as  $11.5 \text{ cm}^{-1}$ .

We emphasize that these conclusions with regard to the

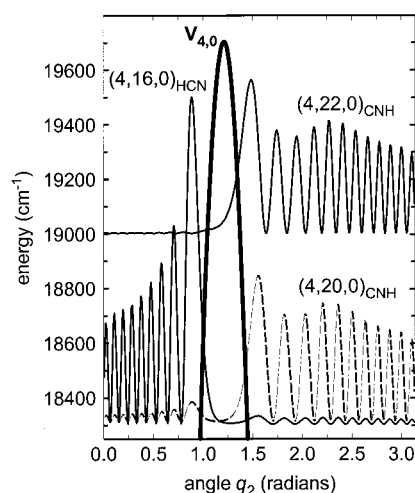


FIG. 4. Plot, as a function of  $q_2$ , of the  $V_{4,0}$  pseudopotential and the probabilities  $|\Psi(q_2)|^2 \sin(q_2)$  for the states  $(4,16,0)_{\text{HCN}}$ ,  $(4,20,0)_{\text{CNH}}$ , and  $(4,22,0)_{\text{CNH}}$ , according to the MCH surface. Energy values on the left-hand scale refer to the plot of  $V_{4,0}$  and are given relative to the quantum ground state.  $(4,16,0)_{\text{HCN}}$ ,  $(4,20,0)_{\text{CNH}}$ , and  $(4,22,0)_{\text{CNH}}$  are computed at 18 303.4, 18 314.9, and 19 001.8  $\text{cm}^{-1}$  above the ground state, respectively, according to the perturbation Hamiltonian in Eq. (2.9). All the probability plots are at the same scale. For each plot, the baseline coincides, on the vertical axis, with the energy of the state.

use of pseudopotentials in order to highlight the importance of tunneling and its role in the mixing of molecular eigenstates are illustrative, and only valid for interpreting the perturbatively obtained wave functions. The inaccuracies in both the potential energy surface and the perturbative energies lead to inaccuracies in the pseudopotentials themselves. Since these are used as a starting point in our analysis, this precludes us from making quantitative statements regarding the role of tunneling for the specific state of the real molecule.

The wave functions for the BGBLD surface have been analyzed along the same lines. The most salient feature of the corresponding pseudopotentials is the fact that the “shoulder” in the CNH well is much less pronounced for this surface than for the MCH one. This is clearly seen when comparing Figs. 2 and 5, the latter one displaying the pseudopotentials  $V_{0,0}$  to  $V_{0,4}$ . It is emphasized that all of the surfaces, which have been calculated after the MCH one, agree with the BGBLD surface regarding the importance of the shoulder.<sup>67,104–106</sup> While the  $V_{v_1,0}$  pseudopotentials are very similar to  $V_{0,0}$ , the  $V_{0,v_3}$  ones acquire in contrast an unexpected oscillatory component as  $v_3$  increases. For values of  $v_3$  greater than 3, wave functions localized in the additional wells are clearly observed. However, this happens in energy and quantum number ranges where no exact quantum levels are reported in Ref. 67 and no comparison with experiment is available. Therefore, no conclusion can be drawn as to whether these oscillations are physically meaningful; they may be an artifact of the BGBLD surface or the perturbation procedure.

The maximum error between calculated and experimentally observed transition energies being smaller than  $82 \text{ cm}^{-1}$  for the 92 rotationless transitions observed up to more than

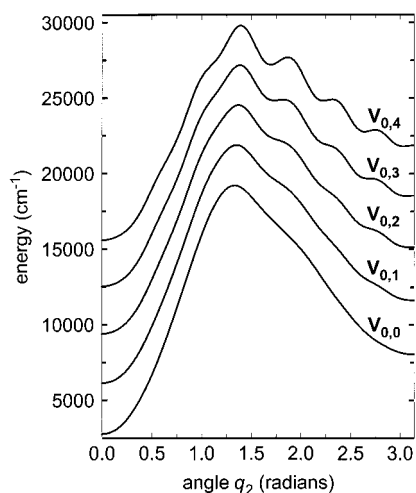


FIG. 5. Plot, as a function of  $q_2$ , of the  $V_{0,0}$ ,  $V_{0,1}$ ,  $V_{0,2}$ ,  $V_{0,3}$ , and  $V_{0,4}$  pseudopotentials, according to the BGBLD surface. Energy values are given relative to the minimum of the potential energy surface.

23 000  $\text{cm}^{-1}$  above the ground state, the precision of the BGBLD surface is good enough to be of use to experimentalists. Therefore, we find it worthwhile to provide simple expressions for calculating the energies of the minima of the HCN and CNH wells and the top of the barrier for different values of  $v_1$  and  $v_3$ . These expressions were obtained from a linear fit to the values calculated from the pseudopotentials and agree on average to better than 2  $\text{cm}^{-1}$  with them. We calculate

$$\begin{aligned}
 E_{\text{HCN}} &= 5.80 + 2067.17I_1 - 7.15I_1^2 + 3473.57I_3 \\
 &\quad + 5.89I_1I_3 - 54.85I_3^2, \\
 E_{\text{CNH}} &= 5173.21 + 2057.11I_1 - 11.65I_1^2 + 3701.70I_3 \\
 &\quad - 31.71I_1I_3 - 45.40I_3^2, \\
 E_{\text{barrier}} &= 16\,861.30 + 2006.77I_1 - 11.62I_1^2 + 2697.52I_3 \\
 &\quad - 4.99I_1I_3 - 10.68I_3^2,
 \end{aligned} \tag{4.3}$$

where the energies are given relative to the bottom of the BGBLD surface and the action integrals  $I_1$  and  $I_3$  are obtained from the quantum numbers  $v_1$  and  $v_3$  according to Eq. (4.1).

### C. Gaps between neighboring levels versus unstable fixed points

As developed in some detail in the work of Svitak, Rose, and Kellman<sup>14</sup> as well as in further studies,<sup>1-4,7,107,108</sup> the plot of energy gaps between levels having two good quantum numbers in common usually displays a clear pattern in the neighborhood of unstable fixed points. In the case of HCN/CNH, one expects that a ‘‘dip’’ (that is, a local minimum) indicates the position of the top of each barrier in the plot of the gaps between neighboring levels with the same values of  $v_1$  and  $v_3$ . It is seen in Fig. 6 that this is indeed the case as long as one does not consider simultaneously the levels localized in the two different wells. More precisely, the bottom plot represents the gaps between neighboring levels with  $v_1$

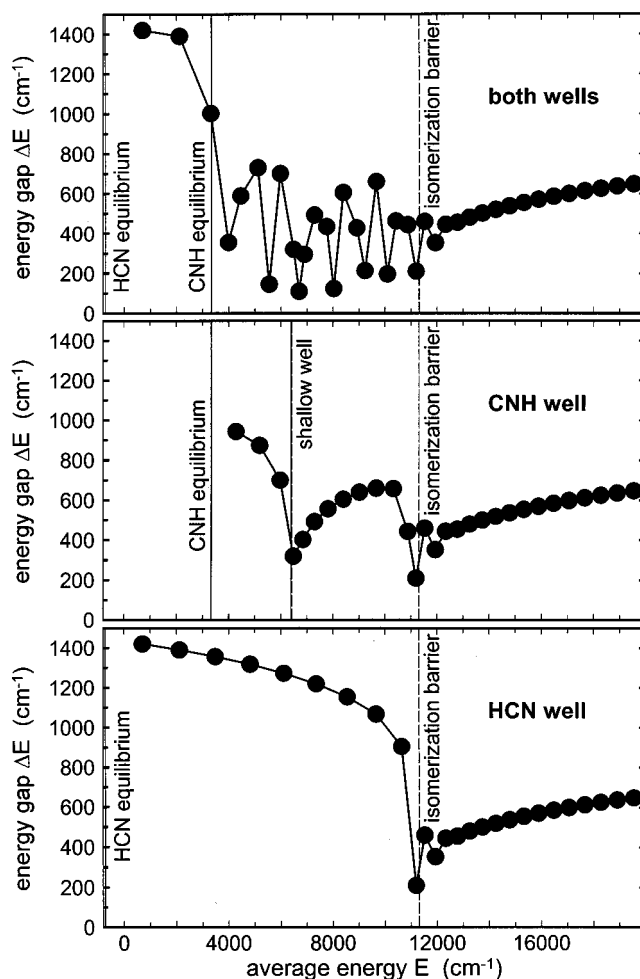


FIG. 6. Plot, as a function of their average energy, of the energy gap between two neighboring states with  $v_1 = v_3 = 0$ . Energy values on the horizontal axis are given relative to the quantum ground state. Bottom plot: The states localized in the CNH well have not been taken into account. Middle plot: The states localized in the HCN well have not been taken into account. Top plot: All the states have been taken into account. The solid and dashed lines in the middle and bottom plots indicate the positions of the minima and maxima of the  $V_{0,0}$  pseudopotential. See Sec. IV C for further explanations.

$= v_3 = 0$  in the MCH surface, where only the states localized in the HCN well and the delocalized states are taken into account. The dip indicates precisely the location of the top of the barrier to isomerization, which is materialized by the vertical dashed line. The fact that the gaps on the high-energy side of the barrier are roughly smaller by a factor of 2 when compared to the low-energy side just reflects the fact that the density of states above the barrier is approximately the sum of the density in each well and the individual densities are similar.

Similarly, the two dips observed in the middle plot, for which the states localized in the CNH well and the delocalized states have been taken into account, coincide precisely with the barrier separating the shallow well from the CNH equilibrium configuration and the barrier to isomerization. Since the states in the two wells are largely uncorrelated, these clear pictures merge into the messy zig-zag pattern observed in the top plot when all of the levels (localized in the HCN well, localized in the CNH well, and delocalized)

are taken into account. Such a zig-zag pattern, arising from the superposition of two clear dips, has also been reported for HCP.<sup>3</sup> Nevertheless, there exists an important difference between the two molecules. Indeed, in the case of HCN, the two sets of levels are separated by a potential barrier, so that it is very easy to put each experimentally observed state in the correct set. In contrast, in the case of HCP, the two sets of levels are separated by a much subtler dynamical separatrix, which makes it difficult to decide whether an observed state belongs to one or the other set of levels.

## V. DISCUSSION

The perturbation Hamiltonian in Eq. (2.9) is the simplest possible one for linear triatomic molecules with two equilibrium positions, because it assumes that the three vibrational modes remain decoupled up to and above the isomerization threshold. In this respect, this Hamiltonian is the counterpart for floppy systems of the well-known Dunham expansion. Despite this simplicity, the eigenstates of the perturbation Hamiltonian agree satisfyingly well with those of the *ab initio* surface obtained from exact quantum calculations. For example, the rms error for all the states up to the isomerization threshold is smaller than  $10\text{ cm}^{-1}$  for the MCH surface. Quite naturally, one might wonder (i) whether it is possible to reduce this error by taking one (or a few) resonance(s) into account, and (ii) which resonance(s) is(are) most important for reducing the error. Neither the Darling–Dennison resonance between the CH and CN stretches suggested in Ref. 92, nor the Fermi resonance between the same degrees of freedom, are likely to play a role in the dynamics of HCN/CNH: Indeed, if they were important, then perturbation theory would diverge at second order,<sup>62</sup> while convergence is observed up to sixth order. In contrast, examination of the states with the largest errors reveals that there probably exists a 1:6 resonance between the CN stretch and the bend. For example, the states  $(0,22,0)_{\text{CNH}}$  and  $(1,16,0)_{\text{CNH}}$  are calculated at  $10\,656.7$  and  $10\,819.8\text{ cm}^{-1}$ , respectively, for the perturbation Hamiltonian, whereas exact values are  $10\,619.8$  and  $10\,850.5\text{ cm}^{-1}$  (errors are  $-36.9$  and  $+30.7\text{ cm}^{-1}$ , respectively). Therefore, it is very likely that a better agreement with exact quantum calculations would be obtained if this particular resonance were taken into account.

However, this calculation does not seem worthwhile. Indeed, the purpose for applying CPT to triatomic molecules, for which exact quantum calculations are now feasible, is certainly not to reproduce the results of exact calculations, *but rather to reveal the principal features of the dynamics of the studied molecules.* The point is that classical or exact quantum calculations performed on the *ab initio* surface do provide lots of details, but are paradoxically unable to give a basic understanding of the studied molecule. Stated in other words, *the two methods are complementary, not competing with one another.* For example, use of an effective Hamiltonian showed that the 1:2 Fermi resonance between the CP stretch and the bend is responsible for all the dynamics of HCP up to 80% of the energy of the isomerization saddle, and in particular for the birth of new wave functions (the so-called “isomerization” states) at about  $13\,000\text{ cm}^{-1}$

above the ground state, which are the precursors of the isomerization reaction.<sup>1–3</sup> Similarly, use of an effective Hamiltonian showed that the 1:2 Fermi resonance between the OCl stretch and the bend is responsible for all the dynamics of HOCl up to 98% of the energy of the dissociation threshold, and in particular for the birth of new wave functions (the so-called “dissociation” states) at about  $14\,000\text{ cm}^{-1}$  above the ground state, which are the precursors of the dissociation reaction.<sup>4</sup> For HCN/CNH, the fundamental result is that the dynamics could hardly be simpler, since the three normal modes remain largely decoupled up to and above the isomerization threshold. This important point remained well hidden behind the intrinsic difficulties of exact quantum calculations. Moreover, such fundamental quantities as the height of the isomerization barrier and of the CNH minimum relative to the HCN minimum for each value of  $v_1$  and  $v_3$  are easily obtained from the 1D bending pseudopotentials [see Eq. (4.3)], whereas there exists no rigorous way for deriving them from the *ab initio* potential energy surface. Last but not least, there has been some controversy as it appeared that the classical phase space of HCN is largely chaotic as low as a few thousands of  $\text{cm}^{-1}$  above the CNH minimum, whereas the quantum wave functions remain much more regular.<sup>109–114</sup> The present work is able to explain this discrepancy by showing that, although chaotic, the *ab initio* Hamiltonian nevertheless remains exceedingly close (an average  $10\text{ cm}^{-1}$  separation) from the separable (and hence completely regular) perturbation Hamiltonian.

Taking the 1:6 resonance between the CN stretch and the bend into account would probably bring perturbation results closer to the quantum ones by a few  $\text{cm}^{-1}$ , but this would also destroy two good quantum numbers, namely  $v_1$  and  $v_2$ . There would remain only one good quantum number left (the number of quanta in the CH stretch degree of freedom), so that the fundamental result that HCN/CNH remains an almost separable system up to and above the isomerization threshold would paradoxically be more difficult to grab—just like in exact quantum calculations!

A last question deals with the applicability of the present method to more complicated systems: How would it work? The answer is that the modified CPT should apply equally well to all the systems with a well-defined minimum energy path linking all the extrema of the surface, and for which all the other singularities of the surface take place at energies much higher than the energy of the isomerization saddle. The question remains obviously open if one of these two conditions is not fulfilled, that is, for example, if there are two “families” of minima with two different MEPs, or if dissociation along one of the coordinates takes place at energies comparable to that of the isomerization saddle. We are currently working on these problems.

## VI. SUMMARY

We have presented a study of the perturbative treatment of the isomerization of HCN/CNH. The treatment requires several significant extensions of the traditional perturbative methods that are designed for dynamics about a single minimum. First the potential was expressed in the appropriate



vibrational coordinates. The stretch–bend coupling was then reduced by deriving a minimum energy path Hamiltonian. The eigenvalues of this Hamiltonian were compared to those of the original Hamiltonian, and excellent agreement was found in both wells. Both classical and quantum mechanical versions of the perturbation theory were presented. The discrepancies in the resulting eigenvalues are due to both quantum corrections and use of Lie transforms versus Birkhoff–Gustavson normal forms. The results of both approaches agree equally well with the variational results, so the classical calculations were used in the majority of the calculations. Finally a key advantage of the perturbative method is that it allows one to interpret the molecular eigenfunctions. We gave several examples of this by constructing pseudopotentials that enable us to elucidate the bending dynamics near the threshold to isomerization.

## ACKNOWLEDGMENT

We are very grateful to Professor Joel Bowman for sending his surface and for kindly answering our questions.

- <sup>1</sup>M. Joyeux, S. Yu. Grebenshchikov, and R. Schinke, *J. Chem. Phys.* **109**, 8342 (1998).
- <sup>2</sup>H. Ishikawa, R. W. Field, S. C. Farantos, M. Joyeux, J. Koput, C. Beck, and R. Schinke, *Annu. Rev. Phys. Chem.* **50**, 443 (1999).
- <sup>3</sup>M. Joyeux, D. Sugny, V. Tyng, M. Kellman, H. Ishikawa, R. W. Field, C. Beck, and R. Schinke, *J. Chem. Phys.* **112**, 4162 (2000).
- <sup>4</sup>R. Jost, M. Joyeux, S. Skokov, and J. Bowman, *J. Chem. Phys.* **111**, 6807 (1999).
- <sup>5</sup>E. L. Sibert and A. B. McCoy, *J. Chem. Phys.* **105**, 469 (1996).
- <sup>6</sup>M. P. Jacobson, C. Jung, H. S. Taylor, and R. W. Field, *J. Chem. Phys.* **111**, 600 (1999).
- <sup>7</sup>J. Bredenbeck, C. Beck, R. Schinke, J. Koput, S. Stamatiadis, S. C. Farantos, and M. Joyeux, *J. Chem. Phys.* **112**, 8855 (2000).
- <sup>8</sup>E. Fermi, *Z. Phys.* **71**, 250 (1931).
- <sup>9</sup>D. M. Dennison, *Phys. Rev.* **41**, 304 (1932).
- <sup>10</sup>I. Suzuki, *J. Mol. Spectrosc.* **25**, 479 (1968).
- <sup>11</sup>J. L. Teffo, O. N. Sulakhina, and V. I. Perevalov, *J. Mol. Spectrosc.* **156**, 48 (1992).
- <sup>12</sup>M. E. Kellman and E. D. Lynch, *J. Chem. Phys.* **85**, 7216 (1986).
- <sup>13</sup>L. Xiao and M. E. Kellman, *J. Chem. Phys.* **93**, 5805 (1990).
- <sup>14</sup>J. Svitak, Z. Li, J. Rose, and M. E. Kellman, *J. Chem. Phys.* **102**, 4340 (1995).
- <sup>15</sup>M. Joyeux, *Chem. Phys.* **221**, 269 (1997).
- <sup>16</sup>M. Joyeux, *Chem. Phys.* **221**, 287 (1997).
- <sup>17</sup>M. Joyeux and L. Michaille, *ACH-Models Chem.* **134**, 573 (1997).
- <sup>18</sup>P. F. Bernath, M. Dulick, R. W. Field, and J. L. Hardwick, *J. Mol. Spectrosc.* **86**, 275 (1981).
- <sup>19</sup>R. Vasudev, *Chem. Phys.* **64**, 167 (1982).
- <sup>20</sup>J. P. Pique, J. Manners, G. Sitja, and M. Joyeux, *J. Chem. Phys.* **96**, 6495 (1992).
- <sup>21</sup>G. Brasen and W. Demtröder, *J. Chem. Phys.* **110**, 11841 (1999).
- <sup>22</sup>M. Joyeux, *Chem. Phys. Lett.* **247**, 454 (1995).
- <sup>23</sup>S. Peyerimhoff, M. Lewerenz, and M. Quack, *Chem. Phys. Lett.* **109**, 563 (1984).
- <sup>24</sup>H. R. Dubal and M. Quack, *J. Chem. Phys.* **81**, 3779 (1984).
- <sup>25</sup>J. E. Baggott, M. C. Chuang, R. N. Zare, H. R. Dubal, and M. Quack, *J. Chem. Phys.* **82**, 1186 (1985).
- <sup>26</sup>C. P. Rinsland *et al.*, *J. Quant. Spectrosc. Radiat. Transf.* **60**, 803 (1998).
- <sup>27</sup>J. M. Flaud and R. Bacis, *Spectrochim. Acta A* **54**, 3 (1998).
- <sup>28</sup>L. Xiao and M. E. Kellman, *J. Chem. Phys.* **90**, 6086 (1989).
- <sup>29</sup>A. D. Bykov, O. V. Naumenko, M. A. Smirnov, L. N. Sinitsa, L. R. Brown, J. Crisp, and D. Crisp, *Can. J. Phys.* **72**, 989 (1994).
- <sup>30</sup>B. T. Darling and D. M. Dennison, *Phys. Rev.* **57**, 128 (1940).
- <sup>31</sup>K. K. Lehmann, *J. Chem. Phys.* **79**, 1098 (1983).
- <sup>32</sup>I. M. Mills and A. G. Robiette, *Mol. Phys.* **56**, 743 (1985).
- <sup>33</sup>J. E. Baggott, *Mol. Phys.* **65**, 739 (1988).
- <sup>34</sup>Z.-M. Lu and M. E. Kellman, *J. Chem. Phys.* **107**, 1 (1997).
- <sup>35</sup>S. Keshavamurthy and G. S. Ezra, *J. Chem. Phys.* **107**, 156 (1997).
- <sup>36</sup>A. Einstein, *Verh. Dtsch. Phys. Ges.* **19**, 82 (1917).
- <sup>37</sup>J. B. Keller, *Ann. Phys. (N.Y.)* **4**, 180 (1958).
- <sup>38</sup>V. P. Maslov and M. V. Fedoriuk, *Semiclassical Approximations in Quantum Mechanics* (Reidel, Dordrecht, 1981).
- <sup>39</sup>E. C. Kemble, *The Fundamental Principles of Quantum Mechanics* (McGraw–Hill, New York, 1939), Sec. 48c.
- <sup>40</sup>J. H. Van Vleck, *Rev. Mod. Phys.* **23**, 213 (1951).
- <sup>41</sup>G. Amat, H. H. Nielsen, and G. Tarago, *Rotation-Vibration Spectra of Molecules* (Dekker, New York, 1971).
- <sup>42</sup>I. Shavitt and L. T. Redmon, *J. Chem. Phys.* **73**, 5711 (1980).
- <sup>43</sup>D. Papousek and M. R. Aliev, *Molecular Vibrational-Rotational Spectra* (Elsevier, Amsterdam, 1982).
- <sup>44</sup>X.-G. Wang and E. L. Sibert, *J. Chem. Phys.* **111**, 4510 (1999).
- <sup>45</sup>X.-G. Wang, E. L. Sibert, and J. M. L. Martin, *J. Chem. Phys.* **112**, 1353 (2000).
- <sup>46</sup>G. D. Birkhoff, *Dynamical Systems*, AMS colloquium (AMS, New York, 1966), Vol. 9.
- <sup>47</sup>F. G. Gustavson, *Astron. J.* **71**, 670 (1966).
- <sup>48</sup>R. T. Swimm and J. B. Delos, *J. Chem. Phys.* **71**, 1706 (1979).
- <sup>49</sup>T. Uzer, D. W. Noid, and R. A. Marcus, *J. Chem. Phys.* **79**, 4412 (1983).
- <sup>50</sup>A. J. Lichtenberg and M. A. Lieberman, *Regular and Stochastic Motion* (Springer, New York, 1983).
- <sup>51</sup>J. R. Cary, *Phys. Rep.* **79**, 129 (1981).
- <sup>52</sup>A. J. Dragt and J. M. Finn, *J. Math. Phys.* **17**, 2215 (1976).
- <sup>53</sup>A. J. Dragt and J. M. Finn, *J. Math. Phys.* **20**, 2649 (1979).
- <sup>54</sup>A. J. Dragt and E. Forest, *J. Math. Phys.* **24**, 2734 (1983).
- <sup>55</sup>G. Hori, *Publ. Astron. Soc. Jpn.* **18**, 287 (1966).
- <sup>56</sup>A. Deprit, *Celest. Mech.* **1**, 12 (1969).
- <sup>57</sup>A. B. McCoy and E. L. Sibert, *J. Chem. Phys.* **95**, 3488 (1991).
- <sup>58</sup>A. B. McCoy, D. C. Burleigh, and E. L. Sibert, *J. Chem. Phys.* **95**, 7449 (1991).
- <sup>59</sup>A. B. McCoy and E. L. Sibert, *J. Chem. Phys.* **92**, 1893 (1990).
- <sup>60</sup>A. B. McCoy and E. L. Sibert, *J. Chem. Phys.* **95**, 3476 (1991).
- <sup>61</sup>E. L. Sibert and A. B. McCoy, *J. Chem. Phys.* **105**, 469 (1996).
- <sup>62</sup>M. Joyeux, *J. Chem. Phys.* **109**, 2111 (1998).
- <sup>63</sup>Y. Pak, E. L. Sibert, and R. C. Woods, *J. Chem. Phys.* **107**, 1717 (1997).
- <sup>64</sup>A. B. McCoy and E. L. Sibert, *J. Chem. Phys.* **97**, 2938 (1992).
- <sup>65</sup>D. Sugny and M. Joyeux, *J. Chem. Phys.* **112**, 31 (2000).
- <sup>66</sup>J. N. Murrell, S. Carter, and L. O. Halonen, *J. Mol. Spectrosc.* **93**, 307 (1982).
- <sup>67</sup>J. M. Bowman, B. Gazdy, J. Bentley, T. J. Lee, and C. Dateo, *J. Chem. Phys.* **99**, 308 (1993).
- <sup>68</sup>B. Gazdy and J. Bowman, *J. Chem. Phys.* **95**, 6309 (1991).
- <sup>69</sup>B. H. Chang and D. Secret, *J. Chem. Phys.* **94**, 1196 (1991).
- <sup>70</sup>K. M. Dunn, J. E. Boggs, and P. Pulay, *J. Chem. Phys.* **85**, 5838 (1986).
- <sup>71</sup>J. P. Brunet, R. A. Friesner, R. E. Wyatt, and C. Leforestier, *Chem. Phys. Lett.* **153**, 425 (1988).
- <sup>72</sup>Z. Bacic and J. C. Light, *J. Chem. Phys.* **85**, 4594 (1986).
- <sup>73</sup>Z. Bacic and J. C. Light, *J. Chem. Phys.* **86**, 3065 (1987).
- <sup>74</sup>J. C. Light and Z. Bacic, *J. Chem. Phys.* **87**, 4008 (1987).
- <sup>75</sup>Z. Bacic, *J. Chem. Phys.* **95**, 3456 (1991).
- <sup>76</sup>B. Gazdy and J. M. Bowman, *Chem. Phys.* **175**, 434 (1990).
- <sup>77</sup>J. A. Bentley, C. M. Huang, and R. E. Wyatt, *J. Chem. Phys.* **98**, 5207 (1993).
- <sup>78</sup>C. Saint-Espès, X. Chapuisat, and F. Schneider, *Chem. Phys.* **159**, 377 (1992).
- <sup>79</sup>X. Chapuisat and C. Saint-Espès, *Chem. Phys.* **159**, 391 (1992).
- <sup>80</sup>C. Saint-Espès, X. Chapuisat, and C. Zuhrt, *Chem. Phys.* **188**, 33 (1994).
- <sup>81</sup>X. Chapuisat, C. Saint-Espès, C. Zuhrt, and L. Zülicke, *Chem. Phys.* **217**, 43 (1997).
- <sup>82</sup>M. Menou and C. Leforestier, *Chem. Phys. Lett.* **210**, 294 (1993).
- <sup>83</sup>F. Gatti, Y. Justum, M. Menou, A. Nauts, and X. Chapuisat, *J. Mol. Spectrosc.* **181**, 403 (1997).
- <sup>84</sup>R. A. Marcus, *J. Chem. Phys.* **45**, 4493 (1966).
- <sup>85</sup>R. A. Marcus, *J. Chem. Phys.* **46**, 959 (1967).
- <sup>86</sup>R. A. Marcus, *J. Chem. Phys.* **49**, 2610 (1968).
- <sup>87</sup>R. E. Wyatt, *J. Chem. Phys.* **51**, 3489 (1969).
- <sup>88</sup>D. G. Truhlar, *J. Chem. Phys.* **53**, 2041 (1970).
- <sup>89</sup>W. H. Miller, N. C. Handy, and J. E. Adams, *J. Chem. Phys.* **72**, 99 (1980).
- <sup>90</sup>S. K. Gray, W. H. Miller, Y. Yamaguchi, and H. F. Schaefer, *J. Chem. Phys.* **73**, 2733 (1980).
- <sup>91</sup>T. Carrington, L. M. Hubbard, H. F. Schaeffer, and W. H. Miller, *J. Chem. Phys.* **80**, 4347 (1984).
- <sup>92</sup>K. K. Lehmann, *Mol. Phys.* **66**, 1129 (1989); erratum **75**, 739 (1992).



- <sup>93</sup>M. Robnik, *J. Phys. A* **17**, 109 (1984).
- <sup>94</sup>N. Moazzen-Ahmadi and I. Ozier, *J. Mol. Spectrosc.* **126**, 99 (1987).
- <sup>95</sup>K. Nakagawa, S. Tsunekawa, and T. Kojima, *J. Mol. Spectrosc.* **126**, 329 (1987).
- <sup>96</sup>O. I. Baskakov and M. A. O. Pashaev, *J. Mol. Spectrosc.* **151**, 282 (1992).
- <sup>97</sup>J. Tang and K. Takagi, *J. Mol. Spectrosc.* **161**, 487 (1993).
- <sup>98</sup>Y.-B. Duan, H.-M. Zhang, and K. Takagi, *J. Chem. Phys.* **104**, 3914 (1996).
- <sup>99</sup>Y.-B. Duan and K. Takagi, *J. Chem. Phys.* **104**, 7395 (1996).
- <sup>100</sup>Y.-B. Duan, Z.-D. Sun, and K. Takagi, *J. Chem. Phys.* **105**, 5348 (1996).
- <sup>101</sup>Y.-B. Duan, L. Wang, and K. Takagi, *J. Mol. Spectrosc.* **193**, 418 (1999).
- <sup>102</sup>J. Schwinger, in *Quantum Theory of Angular Momentum*, edited by L. C. Biedenharn and H. van Dam (Academic, New York, 1965).
- <sup>103</sup>R. Hernandez, *J. Chem. Phys.* **101**, 9354 (1994).
- <sup>104</sup>B. Gazdi and J. M. Bowman, *J. Chem. Phys.* **95**, 6309 (1991).
- <sup>105</sup>J. A. Bentley, J. M. Bowman, B. Gazdi, T. J. Lee, and C. Dateo, *Chem. Phys. Lett.* **198**, 563 (1992).
- <sup>106</sup>Q. Wu, J. Z. H. Zhang, and J. M. Bowman, *J. Chem. Phys.* **107**, 3602 (1997).
- <sup>107</sup>C. Beck, H. M. Keller, S. Y. Grebenshchikov, R. Schinke, S. C. Farantos, K. Yamashita, and K. Morokuma, *J. Chem. Phys.* **107**, 9818 (1997).
- <sup>108</sup>J. Weiss, J. Hauschildt, S. Y. Grebenshchikov, R. Düren, R. Schinke, J. Koput, S. Stamatiadis, and S. C. Farantos, *J. Chem. Phys.* **112**, 77 (2000).
- <sup>109</sup>K. K. Lehmann, G. J. Scherer, and W. Klemperer, *J. Chem. Phys.* **76**, 6441 (1982).
- <sup>110</sup>K. K. Lehmann, G. J. Scherer, and W. Klemperer, *J. Chem. Phys.* **77**, 2853 (1982).
- <sup>111</sup>D. Farrelly and W. P. Reinhardt, *J. Chem. Phys.* **78**, 606 (1983).
- <sup>112</sup>K. K. Lehmann, G. J. Scherer, and W. Klemperer, *J. Chem. Phys.* **78**, 608 (1983).
- <sup>113</sup>M. Founargiotakis, S. C. Farantos, and J. Tennyson, *J. Chem. Phys.* **88**, 1598 (1988).
- <sup>114</sup>S. C. Farantos, J. M. Gomez Llorente, O. Hahn, and H. S. Taylor, *J. Chem. Phys.* **93**, 76 (1990).